DOI: 10.1111/cgf.12715
COMPUTER GRAPHICS *forum*
Volume 35 (2016), number 1 pp. 138–151

Fast ANN for High-Quality Collaborative Filtering

Yun-Ta Tsai[1,2], Markus Steinberger[1,4], Dawid Pająk[1,3] and Kari Pulli[1,3]

[1]NVIDIA, Santa Clara, US
[2]Google Inc. , Mountain View, US
yuntatsai@google.com
[3]Light, Palo Alto, US
{dawid, kari}@light.co
[4]Graz University of Technology, Graz, Austria
steinberger@icg.tugraz.at

Abstract

Collaborative filtering collects similar patches, jointly filters them and scatters the output back to input patches; each pixel gets a contribution from each patch that overlaps with it, allowing signal reconstruction from highly corrupted data. Exploiting self-similarity, however, requires finding matching image patches, which is an expensive operation. We propose a GPU-friendly approximated-nearest-neighbour(ANN) algorithm that produces high-quality results for any type of collaborative filter. We evaluate our ANN search against state-of-the-art ANN algorithms in several application domains. Our method is orders of magnitudes faster, yet provides similar or higher quality results than the previous work.

Keywords: approximated nearest neighborhood, parallel computing, non-local means, denoising

ACM CCS: I.4.3 [Image Processing and Computer Vision]: Enhancement Filtering.

1. Introduction

Noise removal [BCM05, DFKE06] is an important problem in application domains such as imaging, image synthesis and geometry reconstruction (Figure 1). A powerful approach to noise removal relies on self-similarity in the data. Exploiting self-similarity requires finding data points (pixels in 2D images, 3D points in surface scans) that have locally similar patterns of neighbouring values. This matching is often done by considering an image patch, which provides sufficient context to enable robust matches. Overlapping patches also facilitate collaborative filtering: if the image patches are, for example, of size 8×8, each pixel is part of 64 different patches, and if all those are filtered separately, each pixel receives 64 different results. These 64 results can further be filtered or averaged to obtain strongly denoised estimates. Similar patches could be found from nearby regions in the same image, or in a time sequence, from different images. It is often desirable to find several matching patches instead of finding just the single, best match. This problem can be formulated so that the patch is interpreted as a high-dimensional vector (e.g., 64D for 8×8 patches), and the k closest vectors are found in a k-nearest-neighbour (kNN) search. Relaxing the problem by requiring only approximate matches allows significant speed-ups at only a negligible cost on the denoising performance. This leads to a class of algorithms called the approximate-nearest-neighbour (ANN) algorithms.

Many techniques that accelerate ANN search have been proposed. Examples include random KD-trees, K-means clustering, local sensitive hashing and principal component analysis (PCA). While being efficient, the majority of these solutions suffers from (i) the curse of dimensionality, where high-dimensional data become very sparse and the distance metric loses its discrimination power, (ii) limited accuracy, reducing the quality of the matches and the filtering result, (iii) high pre-processing cost, which prohibits the use in interactive applications and (iv) poor performance scaling on massively parallel systems, such as GPUs. Importantly, the search for the best matches is completely separated from collaborative filtering, leading to inefficient implementations.

We present an ANN search method that is optimized for both collaborative filtering and an efficient implementation on the GPU. Whereas many other methods first construct a search structure and then repeatedly use it to perform search and filtering, we in essence perform all the queries in parallel as we construct the

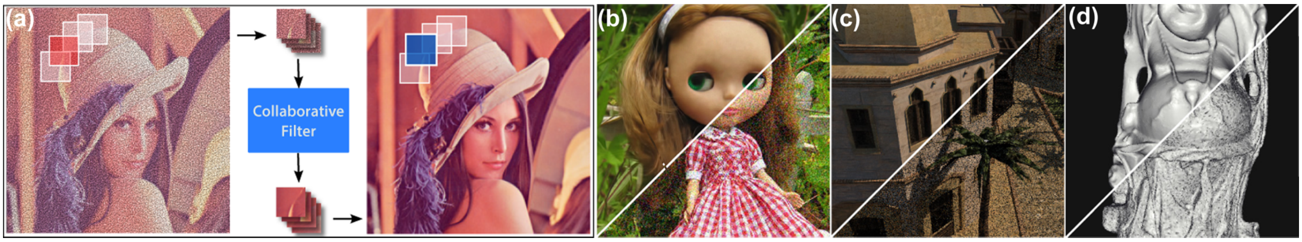

Figure 1: *Collaborative filtering is a powerful, yet computationally demanding denoising approach. (a) Relying on self-similarity in the input data, collaborative filtering requires the search for patches which are similar to a reference patch (red). Filtering the patches, either by averaging the pixels or modifying the coefficients after a wavelet or other transformation, removes unwanted noise, and each output pixel is collaboratively filtered using all the denoised image patches that overlap the pixel. Our method accelerates the process of searching for similar patches and facilitates high-quality collaborative filtering even on mobile devices. Application examples for collaborative filtering include (left: our output; right: noisy input) (b) denoising an image burst, (c) filtering the samples for global illumination and (d) geometry reconstruction.*

search structure. The method is general and can be used in different denoising algorithms. We demonstrate the use of our method for 2D image denoising, both for a single image and an image burst. Furthermore, we show how it can be used to filter the output of ray-traced renderings, and to denoise surfaces recorded with 3D range scanners. This paper is an extended version of a conference paper [TSPP14], and this method was a key enabler for many applications in the FlexISP work [HST*14].

2. Related Work

General high-dimensional filtering has become an important technique in recent years with many interesting applications [AGDL09, GO12]. In this work, we are mostly interested in collaborative filtering [BCM05, DFKE06], which searches for similar candidates in a high-dimensional space.

Zontak and Irani [ZI11] has shown that internal image statistics tends to be more powerful than general external statistics for its predictive power. The likelihood of similar candidates within the same image also drops rapidly with the growth of spatial distance from the patch and its gradient content, which is a powerful prior that can improve the performance of existing collaborative filtering algorithms. Furthermore, combining both internal and external image priors [MZI13] can achieve better result than relying on single prior along.

Regardless which strategy to use, the key enabler for collaborative filtering is a fast nearest-neighbourhood (NN) search; therefore, we focus the discussion here on various NN methods. The *KD-tree* is the most widely used family of algorithms for accelerated NN search [Ben75]. It is very effective for exact search when the data dimensionality is low. For high-dimensional data, several approximations exist.

Randomized KD-trees have been used to look up image features in very large-image recognition problems [PCI*07, SAH08]. To avoid excessive backtracking when searching for neighbouring elements, dynamically built priority queues can be used [AM93, BL97]. Randomized KD-trees address this issue by splitting the data among multiple KD-trees generated from randomized overlapping subsets of the data. The trees are smaller and can be searched concurrently, with less backtracking. Pre-processing becomes more expensive, as the data must first be analysed with PCA to align its moment axes with the coordinate axes of the KD-tree.

There are other methods for mitigating the cost of backtracking. One approach utilizes spatial coherency to *propagate matches* [OA12, HS12]. If the best candidates for a patch have already been found, and a new search is done for a nearby patch, the good matches found previously can be propagated to help the current search. That is, the search just dives into the leaves without backtracking, and also checks the buckets containing the candidates of the neighbour. The bookkeeping of the previous matches adds some overhead, however.

Gaussian KD-trees [AGDL09] sparsely represent distributions in high-dimensional space. They support spatio-temporal filtering, exploit the commonalities between non-local means, bilateral and other related filters based on an assumption of Gaussian distributions, and can be implemented efficiently on the GPU. The key difference to a regular KD-tree is that in addition to the splitting value, it also stores the minimum and the maximum of the data projected onto the cut axis. During search, this can be used to skip branches that are likely to only have few samples. Such design elegantly integrates filtering and NN search into a single data structure. However, it also limits the types of supported filters, whereas our method works with all filters that rely on NN search.

Clustering trees use a different choice for defining how the tree should branch. Fukunaga and Narendra [FN75] proposed *K-means trees*, where a tree structure is constructed via K-means, recursively at each level clustering the data points into k disjoint groups. The trees are constructed by *hierarchical clustering* [ML12], where the branching factor k determines whether a flat or deep tree is built. For clustering, a simple random selection of k points is used. To improve search performance, multiple trees can be built in parallel. Nistér and Stewénius [NS06] proposed to construct trees in the metric space. An advantage of using K-means is its efficiency of clustering. However, the centroid can be easily influenced by outliers. We use the Fast Library for Approximate Nearest Neighbors (FLANN) implementation [ML] as our benchmark k-means tree implementation. K-means trees can also be combined with KD-trees to boost search performance [ML09]. This approach has successfully been adopted for noise reduction [BKC08], where Brox *et al.* perform a recursive k-means clustering with $k = 2$ splits in each node. To increase precision, patches within distance w of a decision boundary are assigned to both sets, which increases the memory footprint and complicates data management.

Vantage point trees [Yia93] split points using the absolute distance from a single centre, instead of partitioning points on the basis of relative distance to multiple centres. The number and thickness of these so-called 'hypershells' can also be chosen in various ways to improve the performance in image processing applications [KZN08].

Locality-sensitive hashing [GIM99] is an efficient method for NN search on binary features. Zitnick [Zit10] proposed a similar method using *mini-hash* for the same purpose. While a binary descriptor has a small-memory footprint and the Hamming distance can be used as an efficient metric, a fairly large support is required to have enough discriminative power, which makes collaborative filtering more costly.

To accelerate search, *PatchMatch* [BSFG09] uses a random NN search where neighbouring patches propagate good matches. The *generalized PatchMatch* [BSGF10] further improves this search strategy to support kNN queries. Liu and Freeman [LF10] extended the concept of random NN search further to video denoising while achieving temporal smoothing result. To avoid brute force search, *PatchGP* [CKYY13], an extension to *pixel geodesic paths* [BS07], only checks subsets of path directions. As the distance measure on these subsets can be unreliable due to noise, PatchGP uses customized multi-scale filters to achieve good denoising results.

Many GPU-accelerated nearest-neighbourhood techniques have been proposed. For instance, redundant norm computations can be minimized by exploiting an overlap between search windows [XLYD11], or accelerated insertion sort [GDNB10]. However, the running times are several times slower than with approximative methods. Pan and Manocha proposed parallelized local sensitive hashing [PM11] with RP-tree and cuckoo hashing. To reduce the search space, the data can also be partitioned into a set of randomly overlapping spheres [Cay10]. If the structure of the data is known, such as 3D points, performance can be further improved [ZHWG08, QMN09, LSP*12, LTF*12]. Combining with accelerated radix sort [MG11], the process of sorting potential candidates can be speeded up significantly.

All these algorithms suffer from one or more of the following problems:

- complex data structures are needed for managing nodes and search,
- dimensionality reduction lowers filtering quality and degrades denoising performance, especially in high-noise scenarios,
- costly pre-processing is required,
- multiple levels of indirection are not well suited for current GPU architectures (*pointer chasing*),
- suboptimal support for collaborative filtering,
- unreliability with high noise.

Our method addresses all of these problems and we demonstrate its benefits in multiple applications.

Table 1: *Comparison of non-local means (NLMs) filtering for the BM3D dataset [DFKE06] using three different search scopes. Each image is corrupted with zero-mean additive Gaussian noise with $\sigma = 20$, peak signal-to-noise ratio (PSNR) = 22.12 dB; patch size 8×8 and number of candidates $k = 16$. Global covers the whole image, Sliding window uses a symmetric search window around each patch's centre and Tile divides the image into non-overlapping tiles within which we look for the patch matches.*

Search scope	PSNR [dB]
Global	28.44
Sliding window (15 × 15)	28.43
Tile (15 × 15)	28.19

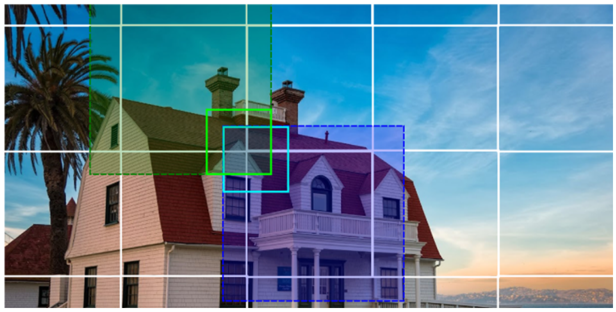

Figure 2: *The implementation of tiled collaborative filtering. The input image is divided into non-overlapping tiles, each $n \times n$ pixels large. Since each patch is centred around a certain pixel within a tile, patches that are close to border of neighbouring tiles (green and blue in the example figure) overlap and contribute to each others filtering results.*

3. ANN for Collaborative Filtering

There are several criteria our ANN method has to fulfill. It should work on images (both 2D colour images and 3D range images or meshes), and be able to handle fairly large patch sizes (e.g., 8×8). Furthermore, the entire method, i.e., the search structure construction, the search and the filtering, needs to be fast. Consequently, the method has to map well on the GPU to benefit from its massive parallelism.

We also want to take advantage of the characteristics of collaborative filtering and known properties of the input data. For example, natural images tend to be locally coherent, both spatially and temporally in case of a video or an image burst. Thus, it is typically sufficient to search for similar image patches in a close proximity [Leb12, BCM05], as a full search over the whole image yields only a small-quality improvement (see Table 1) with a huge increase in the execution time. It is also known that a relatively small number of similar patches/candidates (e.g., $k = 16$) is sufficient [Leb12], and that even this small query can be approximated.

We exploit these characteristics and limit the search space by dividing the image into a set of tiles (see Figure 2). As we demonstrate in Table 1 and Figure 3, for collaborative filtering applications, the tiled search performs almost as well as a full

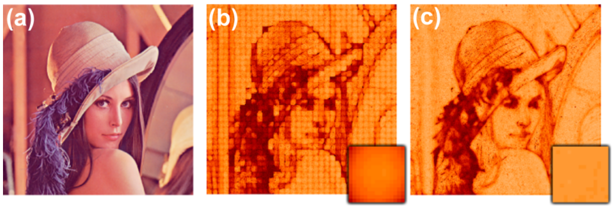

Figure 3: *Average error after denoising with and without patch overlap from neighbouring tiles. (a) Example image from the BM3D dataset [DFKE06] before adding zero-mean Gaussian noise with $\sigma = 20$. (b) When denoising image tiles without patch overlap from neighbouring tiles, pixels close to tile boundaries show higher residual noise than the tile centres. The overlay shows the average residual noise over all tiles. (c) With collaborative filtering across tile borders, the average residual noise is visually uniform over the tile.*

Table 2: *Performance of our method as a function of tile size (BM3D dataset [DFKE06], patch size 8×8, $k = 16$). Each image is corrupted with zero-mean additive Gaussian noise with $\sigma = 20$ that yields PSNR = 22.12 dB. For tiles larger than 15×15 pixels, the improvement in image quality becomes negligible. Increasing the tile size adds to the clustering time, but also decreases the average NN query time due to smaller overall image tile count.*

Tile size	Clustering [ms]	Query [ms]	PSNR [dB]
11 × 11	2.58	2.27	27.65
15 × 15	3.52	2.07	27.79
19 × 19	4.73	1.96	27.82

global or symmetrically centred search. This is because the patches on the border of neighbouring tiles overlap, and therefore contribute to each others filtering results.

To improve the query performance, we pre-cluster patches in a tile so that similar patches are grouped together. While previous methods first construct a search acceleration structure and then repeatedly use the structure to perform a search, we fuse the data structure construction and search, achieving a significant speed-up.

Below, we discuss the main steps of the proposed algorithm: building the cluster list, using it to perform the ANN query and collaborative filtering.

3.1. Pre-clustering patches within a tile

We first divide an image into tiles as shown in Figure 2. Each tile is processed independently during query, but due to the collaborative filtering, the outputs will overlap. A larger tile allows finding better matches, while a smaller tile fits better into the cache or shared memory, maximizing memory locality for each query, as shown in Table 2.

Our preferred setup uses 15×15 tiles (with 225 potential matches) and 8×8 patches. This patch size is a common choice,

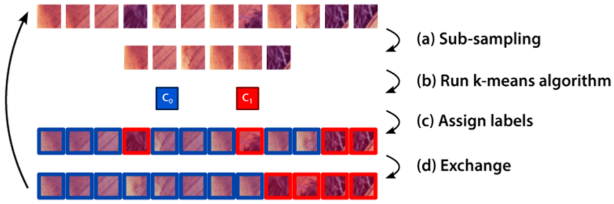

Figure 4: *Hierarchical clustering. (a) The input cluster is subsampled and used to (b) estimate two new cluster centres. (c) The patches in the input cluster are associated with the closest centre, and then (d) reorganized to produce two new sub-clusters. The process is repeated until the output cluster size falls below a certain threshold.*

Table 3: *Impact of the sample count used by K-means clustering on NLM denoising quality (BM3D dataset [DFKE06], 8×8 patches, $k = 16$). Each image is corrupted with zero-mean additive Gaussian noise with $\sigma = 20$, which produces the mean PSNR of 22.12 dB with respect to the original images. Note that with very small cluster size (of 4), the performance degrades due to low occupancy of the GPU.*

Sample count	Clustering [ms]	PSNR [dB]
32	6.40	27.88
16	3.93	27.81
8	3.52	27.79
4	5.71	27.70

as it is large enough to be robust to noise, and small enough for efficient processing [BCM05, DFKE06, Leb12].

The patches are clustered hierarchically (see Figure 4). At each step, the remaining patches (initially all the patches within the tile) are split into two clusters. This is implemented with a variant of K-means++ [AV07] algorithm, which we additionally modified to remove irregular workloads and pseudo-random memory access patterns. The new algorithm performs better on the GPU and is summarized below:

1. Choose the first patch in the node as the first centre.
2. Compute ℓ^2 norm n_i between the first patch and every other patch and normalize the distances with $c_i = \frac{\sum_{j \le i} n_j}{\sum_i n_i}$.
3. The first patch with c_i greater than the threshold τ (we use $\tau = 0.5$) is selected as the second centre.

To speed up the process, we only perform K-means on a subset of patches. To find the cluster centres, we evenly select, for example, eight patches out of all the patches stored in a particular cluster. As we show in Table 3, this sub-sampling only slightly affects the clustering quality, but drastically reduces the computational load. Finally, we assign each patch to the closest of the two centres.

The clustering process continues recursively until the size of the cluster is below a threshold, which usually is twice the number of candidates required for filtering. For instance, for non-local means image denoising, we use the top 16 matches for each patch, in which case we stop the recursion when the cluster is smaller than 32 patches.

Table 4: *Optimization strategies and speed-up for clustering for a* 0.25 *MPix image on a GTX 680.*

Strategy	Time [ms]	Speed-up
Naïve implementation	272.06	–
Warp-wide processing	6.54	41.62×
Persistent thread	4.84	56.16×
Parallel exchange	3.46	78.68×

3.2. Query and candidate refinement

After clustering, we can perform the NN query. Because similar patches are grouped within the same cluster, we do not need to perform a traditional tree traversal; instead, for each patch in the cluster, we simply find its NNs by inspecting the patches in the cluster. If higher quality is required, we can search additional clusters. This increases the query time, which grows quadratically with the number of clusters being searched. However, we found that in most cases, searching a single cluster is sufficient.

Figure 5 illustrates the parallel exhaustive search within a cluster. For each patch, we find the indices of the kNNs within the same cluster. We encode the indices of the NNs as a bit field, if the maximum number of elements in a cluster is 32, a 32-bit integer suffices. Replacing repeated tree searches with a simple cluster lookup results not only in a tremendous speed-up, but also allows us to efficiently implement collaborative filtering.

3.3. Collaborative filtering

After the candidate list is generated, we perform collaborative filtering in parallel for each cluster. For each patch, the NNs are fetched, the stack of matching patches is filtered and the results are distributed to each participating patch in the output image. Since all patches within the same cluster are likely to have some common candidates, locality is maximized and computation can be drastically reduced.

4. Implementation

Several GPU processing models inspired the implementation of our approach. Work queues are an efficient way to recursively construct tree structures on the GPU [CT08, GPM11]. They enable a parallel programming paradigm where multiple producers and consumers can execute tasks in a coherent and thread-safe manner. Each task is associated with a descriptor which stores the range of elements (pixels/patches) that should be processed. The descriptors for to-be-processed tasks are compact and can be stored in the queue in GPU memory. The execution threads run in a loop and consistently draw tasks from the queue until all tasks have been processed. Each task can add new 'child' tasks to the end of the queue. This way of looping until all tasks have been completed is called a *persistent threads approach* [AL09]. In contrast to previous work, which usually employs one thread per task, we use the entire thread *warp*. A warp corresponds to a small group of threads which is executed in lock step on the single instruction, multiple threads (SIMTs) hardware used in GPUs. As we show in Table 4, this strategy significantly increases the performance.

Our algorithm offers opportunities for extensive parallelization. First, each tile can be processed in parallel. Second, the individual splits during hierarchical clustering can be parallelized. Finally, candidates for each query can be determined in parallel. In a CPU implementation, this parallelism can be exploited in a multi-threaded implementation in conjunction with Streaming SIMD Extensions (SSE) vectorization. Using the available parallelism in a GPU implementation faces several additional challenges:

- C1: **Register pressure**. Keeping a local copy of a single high-dimensional input vector may exceed the per-thread register file. Computations such as K-means ultimately lead to spilling registers to slower memory.
- C2: **Memory access patterns**. The clustering algorithm groups unrelated patches to nearby memory locations, leading to inefficient, scattered memory access patterns.
- C3: **Thread divergence**. The number of instructions executed for clustering depends on the data. Threads within the same warp but working on different nodes will show varying execution times and divergence hurts performance.
- C4: **Kernel launch overhead**. Hierarchical clustering is very similar to tree construction. The amount of parallelism close to the root of the tree is too low for efficient GPU execution, constructing a tree level-by-level results in serious kernel launch overheads, and determining efficient thread setups for unbalanced trees requires additional management overhead.
- C5: **Memory footprint**. Computing and storing the candidates for all queries in parallel can result in serious memory and bandwidth requirements when storing the candidate information (particularly important on a mobile System on Chip (SoC)).

We present next an efficient GPU implementation addressing all these challenges.

4.1. Clustering

The input data for our algorithm are given by high-dimensional patch data that usually surround the current pixel (image data) or the current vertex (3D mesh data). Extracting this patch data from the original input representation would significantly increase memory consumption as it duplicates the overlapping input data. Given that the following stage simply clusters similar patches without altering the patch data, we store and work on references (the pixel coordinates). This way, cache hit rates also increase as neighbouring patches access overlapping regions. In video and image stack processing, the data reference can include the frame number; in mesh processing, the vertex index can be used as a reference.

The major workload of clustering is formed by the 2-means algorithm, which is repeatedly run on subsets of the input data to generate a hierarchical clustering. Binary clustering is an inherently diverging and irregular task, both at instruction level and in terms of memory. During clustering, distances between arbitrary patches may be computed. Clustering at thread level would impose several problems mentioned earlier (**C1–C4**). When using one GPU thread to perform the split according to the 2-means algorithm, we cannot expect threads within a warp to access close-by memory in the input data. Thus, memory access patterns are not cache-friendly, leading to suboptimal performance (**C2**). As the runtime of the 2-means

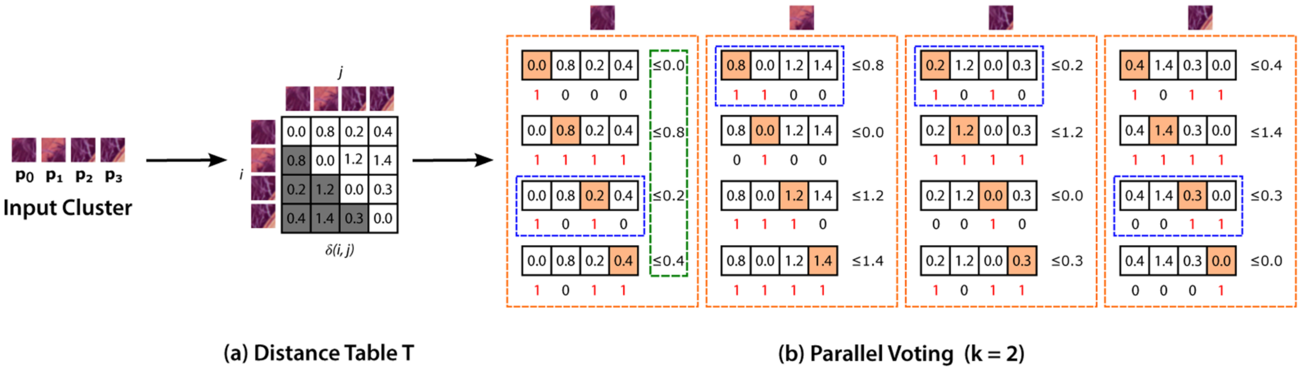

Figure 5: *Cluster-wide KNN lookup. Finding kNNs (here 2) for all patches in a cluster (here 4) is done in two steps. (a) First, we compute a symmetric lookup table T that stores pairwise distances δ between all the patches in the cluster. (b) The voting process for each target patch can be run in parallel (dashed orange box). For each voting process, only the distances to the target patch are of interest ($\delta_{m,0}$ to $\delta_{m,3}$ for patch). We run through all those distances sequentially (green box) and compare how many distances fall below the current distance (red one instead of black zero). If that number matches the target k, the corresponding KNN patches have been found (blue highlight).*

algorithm depends on the initialization, data distribution and number of input elements, different threads are presented with strongly different workloads. This results in the performance decrease due to thread divergence (**C3**).

To address these problems, we developed a warp-wide binary clustering algorithm based on shuffle instructions. Shuffle instructions permit exchange of a variable between threads of the same warp without use of shared memory. This allows us to keep only a subset of the high-dimensional data in each thread, reducing register usage. Furthermore, assigning successive dimensions to the individual threads in the warp automatically leads to good memory access patterns since the input dimensions sit next to each other in memory. Using multiple threads to split a single cluster (node) offers the opportunity to alter the roles of individual threads for the different steps of the *k*-means algorithm. Our warp-wide binary clustering works like this:

1. Each cluster is assigned a warp for splitting it, the first centre is set.
2. For each sub-sampled patch in the cluster, the entire warp computes the distance to the first centre by executing a parallel reduction using efficient shuffle instructions.
3. Each thread keeps one of the computed distances in a register; the warp computes a prefix sum of these distances to choose the second centre.
4. All threads in the warp cooperatively run at most five iterations of the *k*-means algorithm. At each iteration, the two centres are updated, and the distances are re-computed using parallel reductions.
5. The entire warp determines for each patch the distance to both centres for re-assignment.
6. All threads run through the patch array from the front and back at the same time, marking non-fitting pairs for exchange. As soon as the number of pairs to exchange matches the warp size, all threads perform exchanges concurrently.

These steps address both **C1** and **C2**, and also avoid divergence (**C3**), as an entire warp works on the same problem. Also, the problem of low parallelism on the first levels of hierarchical clustering is reduced, as the number of threads working at each level is multiplied by the warp size.

The only remaining issues are the kernel launch overhead and thread setup when creating the hierarchy (**C4**). To mitigate these issues, we use a task queue [CT08] in combination with a persistent threads implementation [AL09]. A similar technique has been used to generate bounding volume hierarchies [GPM11]. In the task queue, we keep identifiers ($lowerIndex$ and $upperIndex$) for each node that still needs to be split. Each worker warp draws such an identifier pair from the queue, splits the corresponding node, puts the identifier for one child back into the queue and starts working on the other child. In this way, only a single kernel launch is needed and nodes at different levels can be worked on concurrently.

The impact of these optimizations is shown in Table 4. Warp-wide execution clearly has the highest impact on the performance, increasing execution speed by a factor of 40. Additionally, avoiding the kernel launch overhead and working on nodes from multiple levels concurrently reduces the execution time by 26%. A further 29% reduction is due to the parallel exchange strategy. Overall, our optimizations reduced execution time by 98.8% compared to a naïve implementation.

4.2. Query

After clustering, similar patches are grouped in the same cluster. The next closest set of patches can be found in the adjacent clusters. This spatial relationship allows us to quickly retrieve potential candidates without costly traversal.

Considering **C1–C2**, we again perform warp-wide computations instead of using a single thread to select the candidates. To determine the candidates for an entire cluster, we use a block of threads. Each warp is then used to compute a set of inter-patch distances. To minimize divergence, each warp is assigned to a cluster. Like with warp-wide binary clustering, we perform warp-wide reduction to compute the norm. Because the distance is symmetrical, we can

Table 5: *Optimization strategies and speed-up for query for a* 0.25 *MPix image on a GTX 680.*

Strategy	Time [ms]	Speed-up
Naïve implementation	171.19	–
Warp-wide processing	10.85	15.78×
No tree	5.86	29.21×
Voting	3.33	51.41×
Compressed candidates	3.17	54.00×

pre-compute all the pairwise distances within a cluster, and store them in shared memory, as illustrated in Figure 5. Each entry $T(i, j)$ stores the value of $\delta_{i,j}$ for patches P_i and P_j.

Once the matrix is computed, each warp is assigned to generate the candidates for a single patch P_s. Instead of sorting all candidates, we follow a voting scheme, which turned out to be nearly twice as fast as sorting: each patch P_i in the cluster is uniquely assigned to one of the threads in the warp. If the cluster size matches the warp size, every thread is responsible for a single patch. We then iteratively try to find the distance threshold λ w.r.t. P_s, which yields k candidates. Because all the possible thresholds are in the matrix, we only iterate over the stored distances. To compute the number of patches that fall within the threshold, we use *ballot* and *popc* instructions. This is the whole process:

1. Each thread block is assigned to a cluster.
2. Compute distance $\delta_{i,j}$ using warp-wide reduction and store the result in $T(i, j)$ and $T(j, i)$.
3. Each warp is assigned to determine the candidates for a single patch P_s.
4. Find at most k patches whose distance to P_s is less than or equal to λ iteratively via voting, where $\lambda = T(i, s)$.

In our algorithm, candidates are only searched for in the same cluster or within two neighbouring clusters with additional expense of shared memory. Thus, all candidate patch references are close in memory after indexing. We can exploit this fact to reduce the memory requirements when encoding the candidates (**C5**). Instead of storing each individual candidate index, we only store the candidate index within the cluster using a bit field. This strategy allows us to use the result of the voting scheme (*ballot* instruction) directly to encode the candidates, reducing the memory requirement to as many bits as there are elements in a cluster.

The impact of this optimization is shown in Table 5. Warp-wide execution again has the highest impact on the performance, speeding up search by a factor of about 16. Avoiding the tree traversal nearly halves the execution time. Another 43% reduction compared to sorting is achieved by the voting scheme. Finally, the compressed candidate encoding reduces execution time by merely 5%. However, this optimization reduces the memory required for candidate encoding by one order of magnitude.

4.3. Filtering

While we only covered clustering and query in more detail, most of these techniques can also be used during the filtering stage that follows the query stage in most applications. When working with patch data, we again use an entire warp to work on a single patch to reduce register pressure and per-thread shared memory requirements. All optimizations reducing data load and store can also be used during filtering.

During collaborative filtering, we take advantage of the grouping of similar patches. Often, steps in collaborative filtering, such as the transformation in BM3D filtering or the distance computations between patches in NLM, can be formulated as pre-computations. Running such pre-computations on the entire input data and storing it in memory is often wasteful, e.g., computing a 2D DCT on every input patch increases memory consumption by the patch dimensions, as all patches need to be stored individually. In our filtering implementations, we start a block of threads for each cluster and run these pre-computations only for the patches in that cluster. Intermediate results can be stored in fast local shared memory. We can also cache the filtering results in this fast memory. After the entire cluster has been filtered, we transform the data back to the original domain and write the data to global memory once.

Our candidate encoding scheme allows further optimizations. In many cases, the same set of candidates is used for multiple patches in a cluster, i.e., if patches b and c are candidates for a and a and c are probably going to be candidates for b. Thus, we can run (at least some) computations only once for all patches that share the same candidate set and use the results for all patches. Due to the bitwise candidate encoding, we can efficiently find equal candidate sets using simple comparisons.

5. Evaluation

We compare our algorithm against other ANN methods, focusing on quality and performance. We break the evaluation into the following tests: (i) NN query, (ii) image quality and (iii) performance. For a fair comparison, we only select well-known algorithms that support kNN queries and work with different collaborative filters. If not specified differently, all tests work on 8×8 patches, and use $k = 16$.

NN query (NNQ). We use two metrics to evaluate the quality of the NNQ. First, we compute the overlap between the delivered kNNs with the ground truth determined via exhaustive search, i.e., how many candidates does the ANN method get right. Second, we compute the ratio between the sum of distances of the delivered candidate patches and the ground truth $D_{\text{ann}}/D_{\text{knn}}$, i.e., by how much does ANN increase the average patch distance. These two metrics characterize how close the result of approximation strategy is to the ground truth. Table 6 shows the results for randomized KD-trees [PCI*07, SAH08], K-means trees [FN75], composite trees [ML], hierarchical clustering [ML09], generalized patch-match [BSGF10] (for meaningful comparisons, we only use translations, not scale or rotation), random ball cover (RBC) [Cay10] and our approach. We used the images from the BM3D dataset [DFKE06] and performed NNQ for each 8×8 patch within every 15×15 tile as our benchmark.

Image quality. To evaluate the effects of ANN search on collaborative filtering, we ran patchwise non-local means filtering

Table 6: *Quality metrics for different ANN methods for the BM3D dataset. Our approach returns almost 40% of the NNs. The average distance of the patches returned by our method is 32% worse than the ground truth. RBC gives good results, but its total execution time is over 1000× longer.*

Method	% of correct	$D_{\text{ann}}/D_{\text{knn}}$
Randomized KD-trees	24.87	3.01
K-means	34.86	2.00
Composite	35.21	1.99
Hierarchical clustering	7.18	7.38
Generalized patch-match	0.22	23.91
RBC	97.88	1.01
Ours	39.01	1.32

Table 7: *Average PSNR for 11 images [DFKE06] corrupted with zero-mean Gaussian noise with $\sigma = 20/255$. Patchwise NLM and BM3D filtering use different ANN methods.*

Method	NLM [dB]	BM3D [dB]
Randomized KD-trees	26.88	30.72
K-means	27.13	30.68
Composite	27.02	30.57
Hierarchical clustering	25.65	29.87
Generalized patch-match	21.24	28.92
RBC	27.83	30.71
Ours	27.79	31.05
Exhaustive search (GT)	28.55	31.10

[BCM05] and BM3D filtering [DFKE06] on the dataset from Dabov *et al.* [DFKE06]. We added zero-mean additive Gaussian noise with $\sigma = 20/255$ to the 8-bit data values. We then ran the ANN algorithms on these input images in tiles and collaboratively filtered the returned candidates as in NNQ evaluation. The results are shown in Table 7. Our method is only slightly worse than RBC, and maintains the highest performance among all ANN methods with BM3D. Note that our method achieves a higher PSNR value than RBC for BM3D filtering. This is because our approximation is less likely to match noise to noise. We also tested with and without searching the neighbouring two clusters, as mentioned in Section 3.2; the improvement was modest (0.1 dB), and the cost is quadratic. Thus, all the evaluations only consider a single cluster during query.

Performance. As most ANN approaches require pre-processing, we measure and report the times for both clustering and query on an Intel i7-950 with 8 GB of RAM and an NVIDIA Geforce GTX 680. The FLANN CPU implementations are optimized with multi-threading, and the window search uses SIMD (SSE2). The input resolution is 0.25 MP, and $k = 16$ candidates are to be retrieved for each pixel.

The results of this test are shown in Table 8. The runtimes of all four FLANN implementations (KD-trees, K-means, composite and hierarchical clustering) are very similar. The time is split fairly evenly between pre-processing and query. All four CPU methods deliver their results in about a second, indicating that the implementations are very similar, only the clustering criteria change. Generalized patch-match does not do any pre-clustering, and thus, takes nine times longer for queries. However, by using information from neighbouring pixels to guide the query process, it is about four times faster than a brute force window search. Implementing the same brute force window search on the GPU, the entire query process is done in less than 600 ms, faster than any approach on the CPU. Applying the same optimization strategies for the window search as we used for our approach (warp-wide execution, voting instead of sorting), we lowered the execution time by 90%. However, our approach is still six times faster, completing clustering in 3.6 ms and query in 4.6 ms. Our approach takes less than 1% of the execution time of the fastest CPU implementation.

Table 8: *Runtime for different NN methods. Our method is significantly faster than other methods while still delivering high-quality results.*

Method	Clustering	Query	Total [ms]
Randomized KD-trees	407.00	380.00	788.00
K-means	670.00	312.00	982.00
Composite	666.00	357.00	1024.00
Hierarchical clustering	415.00	601.00	1017.00
Generalized patch-match	0.00	8930.00	8930.00
Window search (CPU)	0.00	36700.00	36700.00
kNN-Garcia (GPU)	25466.00	398.00	26359.00
RBC (GPU)	10837.00	491.00	11328.00
Window search (GPU)	0.00	594.99	594.99
Window search (GPU opt)	0.00	48.30	48.30
Ours (GPU)	3.55	4.64	8.19

We compared our method against two other GPU-based ANN methods: kNN-Garcia [GDNB10] and RBC [Cay10]. Unlike our approach, these methods are not designed to work on small tiles and therefore struggle to perform in this mode (see Table 8). Disabling tiled processing significantly improves their runtime performance—kNN-Garcia took 590.73 ms to complete, and RBC finished in 2565 ms. These numbers, however, are still far from our results. Moreover, a large input patch-set greatly reduces the ANN quality. In case of RBC, disabling tiled processing caused ANN accuracy drop from 97.88% to 33.49%.

We also implemented our algorithm for different architectures. Running on the CPU (Core i7-950), it takes 130 ms to retrieve 16 candidates for 0.25 MPix images. On a mobile GPU (Tegra K1), it takes 122.3 ms, which is even less than the desktop CPU version. Furthermore, our method has a small-memory footprint. For a 0.25 MP image, we only require 5 MB of additional storage. As we can process the image in tiles, we can keep the memory requirement constant while supporting arbitrary image sizes. We can increase the number of concurrently processed tiles for future GPU architectures, which may require a higher workload.

6. Applications

We demonstrate our method for several applications in image processing, global illumination and geometry refinement.

Table 9: *Comparison between the original CBM3D implementation [DFKE06] and our GPU-enabled methods. While our BM3D implementation loses only 0.1 dB in terms of quality, it is more than 1000 times faster. Further improvement in runtime can be achieved by switching to a simpler filter-like NLM filter (at the cost of reduced denoising performance).*

	PSNR [dB]	Runtime [ms]
Input	18.58	–
CBM3D	30.44	812000
Our BM3D	30.34	703
Our NLM	25.75	39

Single-frame noise reduction. It is the primary motivation for many collaborative filtering techniques. Many ANN and acceleration methods have been proposed for this domain, but they either have to rely on additional post-processing to improve the quality [CKYY13] or work only in conjunction with a limited number of filters [AGDL09]. Our method is independent of the choice of filters, while providing consistent quality without additional post-processing. In Table 9, we compare our method against the original CBM3D implementation using their dataset [DFKE06]. Again, we added zero-mean Gaussian noise with $\sigma = 20/255$ to all images. For a fair comparison, both CBM3D and ours are configured to use a discrete cosine transform as the 2D transform, the Walsh–Hadamard transform in the third dimension, and operate in opponent colour space. The only difference is that CBM3D uses a brute-force window search. Our candidate list encoding (Section 4.2) enables us to implement filtering very efficiently on the GPU. The results show that our method is very close to the original implementation, yet significantly faster.

Burst noise reduction. Current digital cameras can operate in a *burst mode* where they quickly capture multiple frames. Simple accumulation of frames from such a burst stack can significantly reduce the noise and improve the overall SNR. The upper bound of this improvement is proportional to $\sqrt{N}$, where N is the stack size. This approach, however, fails for scenes with motion, where naïve accumulation produces visible ghosting artefacts. To mitigate this issue, we perform single-frame denoising, but look for similar patches not only in the spatial, but also in the temporal neighbourhood [DFE07]. This requires a slight modification of the clustering part of our algorithm, which now processes the data at a particular tile location from all frames at once. Then, we perform non-local means filtering for each patch from the reference image. In Figure 6, we compare our method to Gaussian KD-Trees [AGDL09], which support both burst noise reduction and GPU acceleration. For single-frame denoising, Gaussian KD-trees and our approach achieve similar PSNR values, while ours is more than 1500 times faster. For an entire burst stack, our implementation achieves a 3 dB better PSNR while being 2000 times faster. Denoising an entire burst stack is a difficult task for Gaussian KD-trees, as the data become high-dimensional and require PCA pre-processing. As Gaussian KD-trees require multiple parameters to be set and have a very long running time, tuning the approach for optimal image quality is a difficult process.

Global illumination. Many modern interactive global illumination techniques apply guided noise reduction on sparsely sampled indirect illumination [BEM11]. We verify the applicability of our ANN method by using the output from a direct illumination forward rendering pipeline as guidance for performing NN query. Clustering is done on the guidance image only, using an 8×8 patch size. To enhance clustering stability in the shadow regions, we increase the ambient light in the scene. During query, we operate on the guidance data, but return samples from the indirect illumination, which we combine with direct illumination to generate the final result. Results are summarized in Figure 7.

Geometry denoising. Range data produced by 3D scanners are usually noisy and require post-processing [LPC*00]. Self-similarity in the scan data can also be used to reduce this noise. Gaussian KD-trees, in conjunction with NLM filtering, have been used for this task [AGDL09], extracting a detail layer of the mesh after applying Laplacian smoothing. To evaluate the suitability of our ANN algorithm, we replaced Gaussian KD-trees with our approach to generate filtering candidates. The results of this evaluation are shown in Figure 8.

Joint image upscaling and denoising. Recently introduced image upscaling algorithms [FF11, YLC13] exploit local patch-level self-similarity to improve the apparent resolution of images and videos. These methods produce remarkable results as long as the input data are of good quality. For noisy images, such as those produced by mobile cameras, the reconstruction quality decreases significantly (see Figure 9b). This is because the noise in the image is considered a texture and is upscaled together with the underlying image content. To amend the image quality, denoising can be applied before upscaling (Figure 9c). This pre-mature denoising, however, does not remove all the noise, and may compress details that the upscaling method would need.

To address these issues, we fuse NLM denoising with the upscaling algorithm based on a variant of Yang *et al.*'s method [YLC13]. This method iteratively increases the resolution by non-dyadic ratios, e.g., 5:4, and at each iteration performs two basic steps. First, we use a bicubic filter to generate an initial high-resolution estimate, which is then refined by adding a *hallucinated* high-resolution Laplacian band. For small upscaling ratios, many patches in the input image exhibit local self-similarity, i.e., they are cropped versions of their upscaled selves. This property allows us to reconstruct the high-resolution Laplacian patch simply by copying it from the Laplacian of the low-resolution input. The copying involves a small local search (e.g., 3×3 pixels) as we want to copy from a location where both the initial estimate and the input image look alike. We can repeat this procedure for all the pixels in the image to produce a complete approximation of high-resolution Laplacian.

We have modified this algorithm in two significant ways. First, prior to the bicubic upscaling stage, we apply a strong NLM denoising on the input image. This filtering step removes most of the input noise and prevents the bicubic filter from treating it as a texture. Second, for the low-resolution Laplacian band generation, we use the noisy input image and allow the reconstruction algorithm to use more than one candidate ($k = 16$) for the high-resolution Laplacian

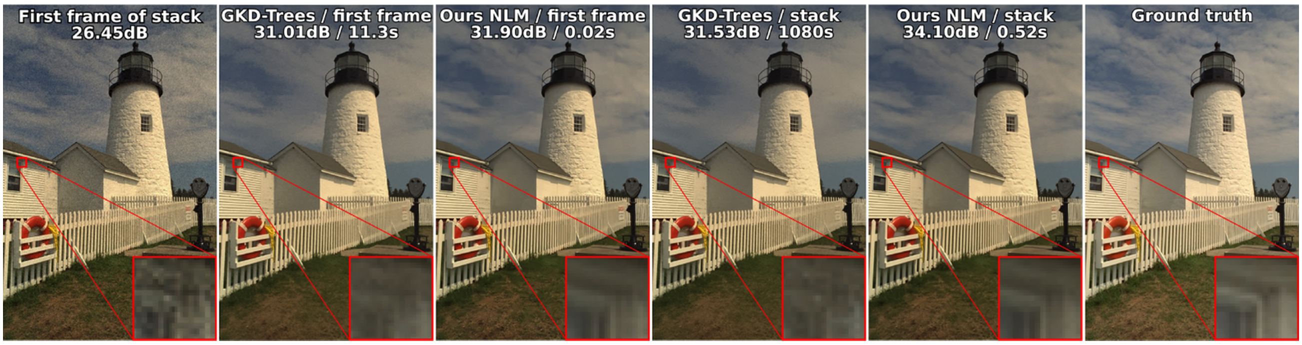

Figure 6: *Burst image denoising. The fence dataset (16 images) was corrupted with additive Gaussian noise of $\sigma = 12/255$. Each frame in the stack is 1.4 MP with random warping to simulate camera motion. Both Gaussian KD-trees and ours run on the same GPU. Parameters for both methods are adjusted for the best image quality. We measured end-to-end processing time from clustering, query and filtering on a GTX 680. Notice that our method significantly outperforms Gaussian KD-trees in both cases.*

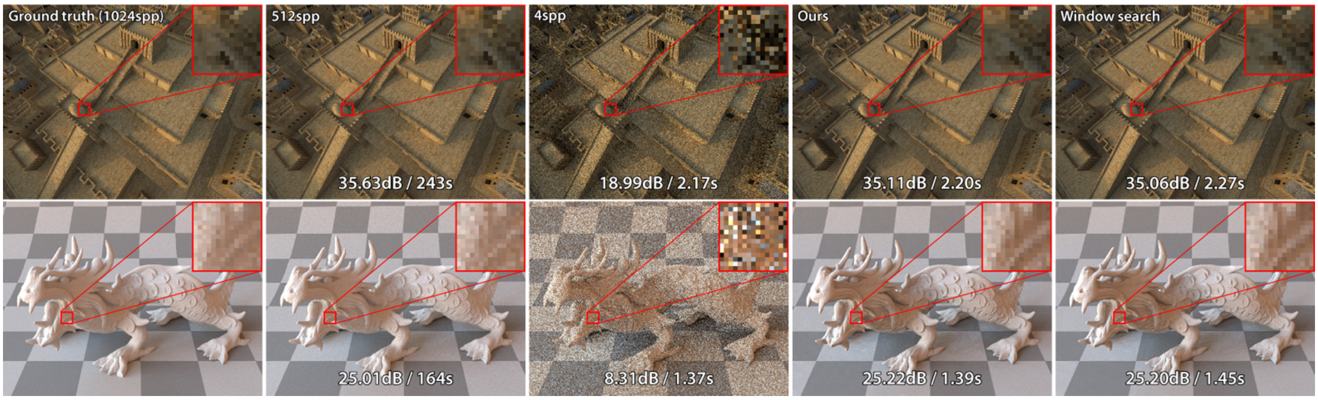

Figure 7: *Global illumination reconstruction. ANN methods can be used to speed up the filtering of noisy Monte-Carlo global illumination rendering. Our ANN method achieves nearly the same quality as window search. In terms of PSNR, both approaches are similar to a 512spp rendering.*

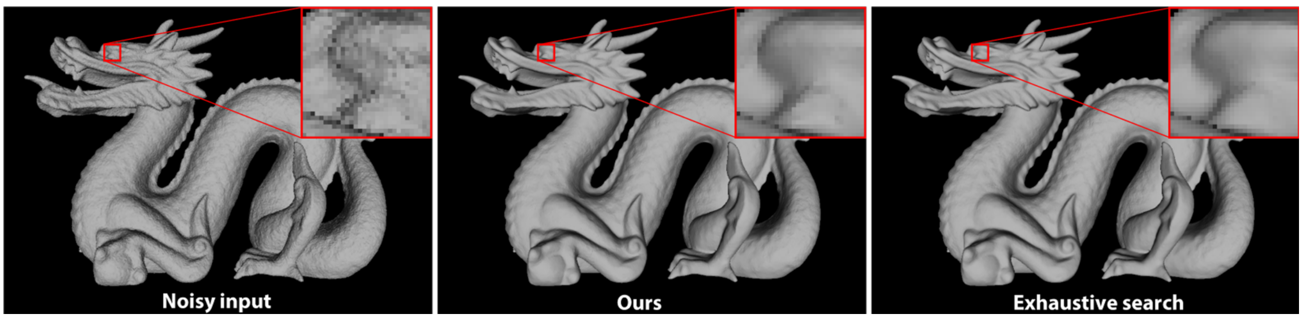

Figure 8: *Geometry denoising. Our ANN algorithm can also be used to find candidates for NLM filtering 3D meshes. Noisy input is generated with σ set to half of the average edge length. The reconstructions of our method and exhaustive search with $k = 256$ are visually indistinguishable.*

patch. We weight these patches using the NLM weighting scheme to produce a high-quality and noise-free estimate of image details. The entire procedure can be repeated in subsequent iterations to yield a stronger noise suppression. In our experiments, however, we found that it is sufficient to denoise the input and corresponding Laplacian in the first iteration only. We demonstrate the upscaling quality of the proposed approach in Figure 9(d). As in previous applications, our ANN algorithm generates results visually indistinguishable from naïve window search (Figure 9e) method while being orders of magnitude faster.

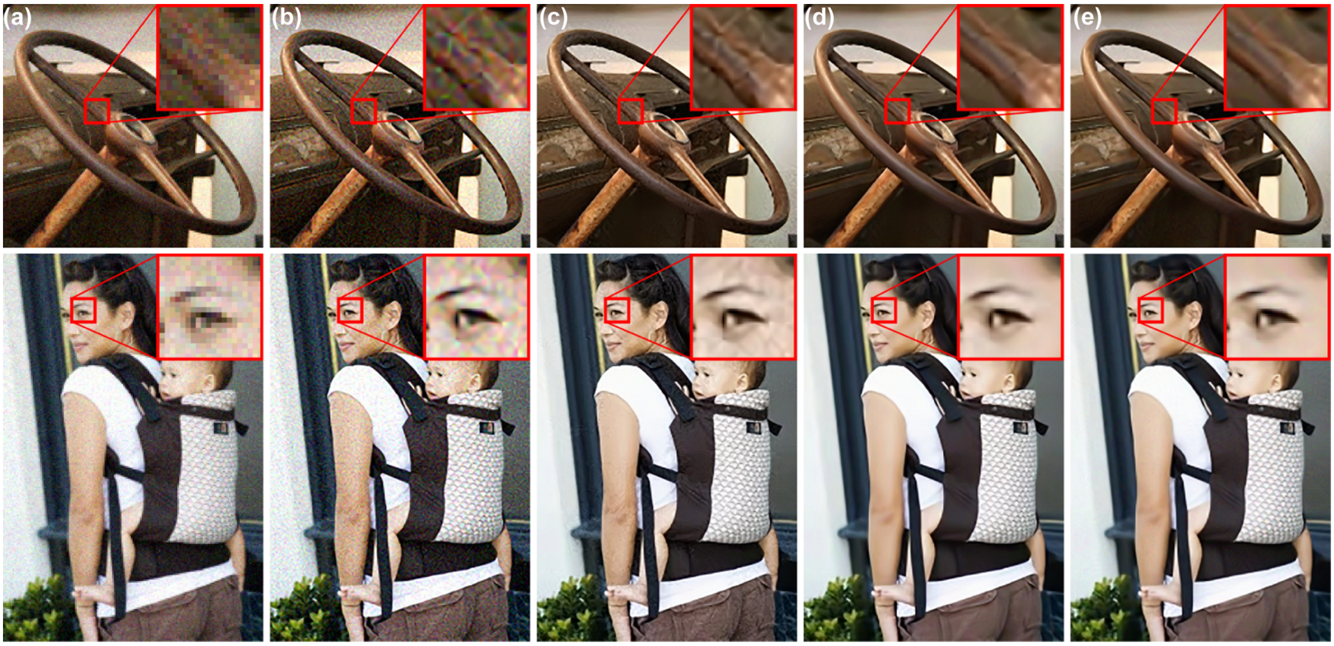

Figure 9: *An example of joint noise reduction and 2× upscaling. (a) Input low-resolution and noisy images (Gaussian noise of $\sigma = 10$). (b) Directly upscaling such images produces unappealing results as noise is interpreted as image structure. (c) Denoising with NLM prior the upscaling improves the quality; however, some residual in the low-resolution input remains and gets amplified during the upscaling. (d, e) Fused denoising and upscaling removes most of the noise without affecting image features important for the upscaling. The results generated with FastANN (d) method are visually indistinguishable from naïve window search (e).*

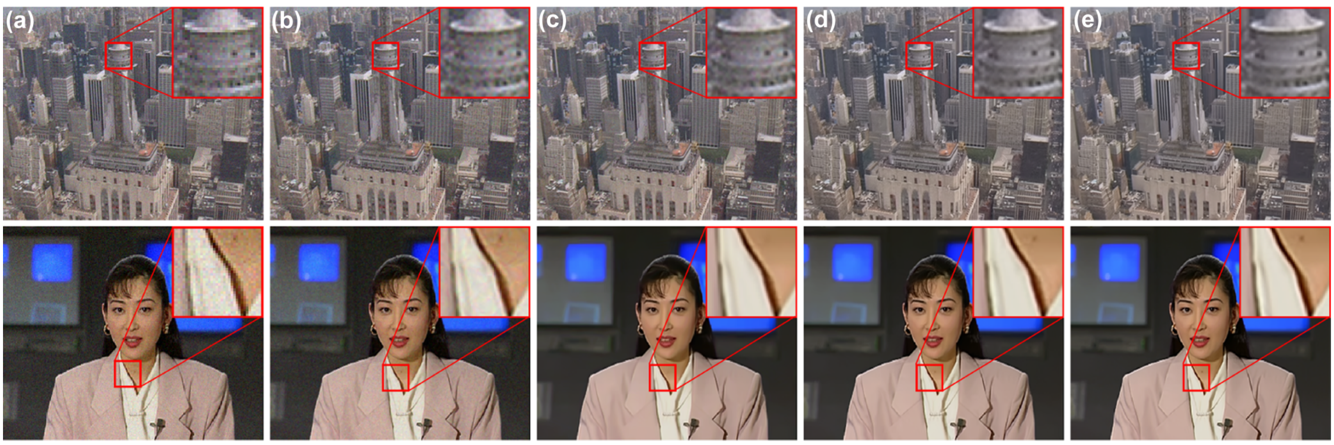

Figure 10: *Joint noise reduction and 2× upscaling for videos. (a) Input low-resolution and noisy video sequences (Gaussian noise of $\sigma = 10$). (b) Directly upscaling frames produces unappealing results as noise is interpreted as image structure. (c) Joint denoising and upscaling in spatial domain, with a search window of 5×5. Some compression and chroma noise artefacts remain. (d, e) Joint denoising and upscaling in spatio-temporal domain, with a search window of 2×2, removes most of the artefacts while preserving small details, such as moles on the skin. (d) Temporal window of ± 2 frames. (e) Temporal window of ± 4 frames.*

Joint video upscaling and denoising. Our method can be further extended to support spatio-temporal upscaling. Although several video upscaling algorithms have been proposed [LS11, DFKE08], finding similar patches in both temporal and spatial domain can be quite time-consuming. However, because consecutive video frames are often highly correlated, extending candidate search to temporal dimension can result in better matched patches. With a stationary camera, we can even reduce the search radius, as good candidates are available at similar image locations in neighbouring frames. Our approach makes joint video upscaling and denoising feasible.

The proposed video upscaling method combines our joint image upscaling and denoising algorithm with burst denoising. Instead of searching for matching patches only in the input image, we extend the search to include data from the adjacent frames. Like with joint upscaling and denoising, we first perform strong NLM denoising on the individual image frames, followed by a bicubic upscaling on all frames. Next, we use the data from all the frames to reconstruct the Laplacian image containing high-frequency details of the current frame. Due to high temporal coherence of the video data, we expect image features to change smoothly in time. Therefore, searching around the same location within ± 5 frames temporal neighbourhood gives us additional well-matched candidates, which we can use to recover lost details, even if individual frames have been corrupted with noise. Obviously, the computational complexity of this operation increases linearly with the number of frames included in the search. The final high-resolution video frame is produced by adding up the reconstructed Laplacian to the upsampled input frame.

To increase the upscaling factor, the same algorithm can be applied iteratively on the output of the previous run. Each iteration increases the number of required images, e.g., the second iteration uses ± 5 upscaled frames in the temporal domain, whereas each of them already required ± 5 at the lowest resolution. Due to high computational overhead, such an upscaling scheme could possibly be used in an offline pre-processing step. Our experiments show that reducing the temporal search radius for successive iterations did not degrade the perceived image quality.

For online video upscaling, we consider a single iteration of our algorithm for which we only need to keep the previous x frames for all scale factors in memory. Figure 10 demonstrates the results on two standard super-resolution datasets.

7. Summary and Conclusions

We have presented an ANN method building on the combination of tiling, hierarchical clustering using 2-means and query within a single cluster. According to our evaluation, our approach can be used as input for high-quality, state-of-the-art collaborative filtering in multiple application domains, such as denoising, super-resolution, burst imaging, global illumination post-processing, geometry reconstruction and image upscaling. Our approach allows for significant GPU acceleration, with only a minimal quality reduction compared to exhaustive search.

Using warp-wide execution (instead of single threads) to work on a patch, avoiding kernel launches, and dynamically changing the work assignment for threads, results in speed-ups between 54× and 79× compared to a naïve GPU implementation. Compared to state-of-the-art ANN methods, we achieve significantly better approximations to the ground truth exhaustive search while being up to 100 times faster. Compared to Gaussian KD-trees [AGDL09] another GPU-based method, we are up to 2000× faster while achieving better image quality.

While our method is designed to work with any collaborative filtering approach, our implementation enforces some restrictions. Our implementation works very well in certain parameter ranges, e.g., patch size 4×4, 8×8 or 16×16. Parameter setups that conflict with the GPU warp size or require too much shared memory can reduce the performance by up to an order of magnitude. In the future, we want to explore the acceleration of complex computation chains where collaborative filtering is the bottleneck, such as end-to-end camera pipelines, video processing and image editing.

References

[AGDL09] Adams A., Gelfand N., Dolson J., Levoy M.: Gaussian KD-trees for fast high-dimensional filtering. *ACM TOG 28*, 3 (2009), 21:1–21:12.

[AL09] Aila T., Laine S.: Understanding the efficiency of ray traversal on GPUs. In *Proceedings of HPG* (2009).

[AM93] Arya S., Mount D.: Algorithms for fast vector quantization. In *Proceedings of Data Compression Conference* (1993).

[AV07] Arthur D., Vassilvitskii S.: k-Means++: The advantages of careful seeding. In *Proceedings of SODA* (2007).

[BCM05] Buades A., Coll B., Morel J.-M.: A non-local algorithm for image denoising. In *Proceedings of CVPR* (2005).

[BEM11] Bauszat P., Eisemann M., Magnor M.: Guided image filtering for interactive high-quality global illumination. *Computer Graphics Forum 30*, 4 (2011), 1361–1368.

[Ben75] Bentley J. L.: Multidimensional binary search trees used for associative searching. *Communications of the ACM 18*, 9 (1975), 509–517.

[BKC08] Brox T., Kleinschmidt O., Cremers D.: Efficient nonlocal means for denoising of textural patterns. *IEEE Transactions on Image Processing 17*, 7 (2008), 1083–1092.

[BL97] Beis J., Lowe D.: Shape indexing using approximate nearest-neighbour search in high-dimensional spaces. In *Proceedings of CVPR* (1997).

[BS07] Bai X., Sapiro G.: A geodesic framework for fast interactive image and video segmentation and matting. In *Proceedings of ICCV* (2007).

[BSFG09] Barnes C., Shechtman E., Finkelstein A., Goldman D. B.: PatchMatch: A randomized correspondence algorithm for structural image editing. *ACM Transactions on Graphics 28*, 3 (2009), 24:1–24:11.

[BSGF10] Barnes C., Shechtman E., Goldman D. B., Finkelstein A.: The generalized PatchMatch correspondence algorithm. In *Proceedings of ECCV* (2010).

[Cay10] Cayton L.: A nearest neighbor data structure for graphics hardware. In *Proceedings of the International Workshop on Accelerating Data Management Systems Using Modern Processor and Storage Architectures* (2010).

[CKYY13] Chen X., Kang S. B., Yang J., Yu J.: Fast patch-based denoising using approximated patch geodesic paths. In *Proceedings of CVPR* (2013).

[CT08] Cederman D., Tsigas P.: On dynamic load balancing on graphics processors. In *Proceedings of the Symposium on Graphics Hardware* (2008).

[DFE07] Dabov K., Foi A., Egiazarian K.: Video denoising by sparse 3d transform-domain collaborative filtering. In *Proceedings of EUSIPCO* (2007).

[DFKE06] Dabov K., Foi A., Katkovnik V., Egiazarian K.: Image denoising with block-matching and 3d filtering. In *Proceedings of SPIE Electronic Imaging* (2006).

[DFKE08] Danielyan A., Foi A., Katkovnik V., Egiazarian K.: Image and video super-resolution via spatially adaptive block-matching filtering. In *Proceedings of International Workshop on Local and Non-Local Approximation in Image Processing (LNLA)* (2008).

[FF11] Freedman G., Fattal R.: Image and video upscaling from local self-examples. *ACM TOG 30*, 2 (2011), 12:1–12:11.

[FN75] Fukunaga K., Narendra P. M.: A branch and bound algorithm for computing k-nearest neighbors. *IEEE Transactions on Computers C-24*, 7 (1975), 750–753.

[GDNB10] Garcia V., Debreuve E., Nielsen F., Barlaud M.: K-nearest neighbor search: Fast GPU-based implementations and application to high-dimensional feature matching. In *Proceedings of ICIP* (2010).

[GIM99] Gionis A., Indyk P., Motwani R.: Similarity search in high dimensions via hashing. In *Proceedings of VLDB* (1999).

[GO12] Gastal E. S., Oliveira M. M.: Adaptive manifolds for real-time high-dimensional filtering. *ACM TOG 31*, 4 (2012).

[GPM11] Garanzha K., Pantaleoni J., McAllister D.: Simpler and faster hlbvh with work queues. In *Proceedings of HPG* (2011).

[HS12] He K., Sun J.: Computing nearest-neighbor fields via propagation-assisted KD-trees. In *Proceedings of CVPR* (2012).

[HST*14] Heide F., Steinberger M., Tsai Y.-T., Rouf M., Pajak D., Reddy D., Gallo O., Liu J., Heidrich W., Egiazarian K., Kautz J., Pulli K.: FlexISP: A flexible camera image processing framework. *ACM TOG 33*, 6 (2014), 231:1–231:13.

[KZN08] Kumar N., Zhang L., Nayar S. K.: What is a good nearest neighbors algorithm for finding similar patches in images? In *Proceedings of ECCV* (2008).

[Leb12] Lebrun M.: An analysis and implementation of the BM3D image denoising method. *Image Processing on Line 2* (2012), 175–213. doi:10.5201/ipol.2012.l-bm3d.

[LF10] Liu C., Freeman W. T.: A high-quality video denoising algorithm based on reliable motion estimation. In *Proceedings of ECCV* (2010).

[LPC*00] Levoy M., Pulli K., Curless B., Rusinkiewicz S., Koller D., Pereira L., Ginzton M., Anderson S., Davis J., Ginsberg J., Shade J., Fulk D.: The digital michelangelo project: 3D scanning of large statues. In *Proceedings of SIGGRAPH* (2000).

[LS11] Liu C., Sun D.: A Bayesian approach to adaptive video super resolution. In *Proceedings of CVPR* (2011).

[LSP*12] Li S., Simons L., Pakaravoor J. B., Abbasinejad F., Owens J. D., Amenta N.: kANN on the GPU with shifted sorting. In *Proceedings of HPG* (2012), 39–47.

[LTF*12] Leite P., Teixeira J. M., Farias T., Reis B., Teichrieb V., Kelner J.: Nearest neighbor searches on the GPU. *International Journal of Parallel Programming 40*, 3 (2012), 313–330.

[MG11] Merrill D., Grimshaw A.: High performance and scalable radix sorting: A case study of implementing dynamic parallelism for GPU computing. *Parallel Processing Letters 21*, 2 (2011), 245–272.

[ML] Muja M., Lowe D. G.: Flann - fast library for approximate nearest neighbors. Accessed: December 2013. http://www.cs.ubc.ca/research/flann/.

[ML09] Muja M., Lowe D. G.: Fast approximate nearest neighbors with automatic algorithm configuration. In *Proceedings of VISAPP* (2009).

[ML12] Muja M., Lowe D. G.: Fast matching of binary features. In *Proceedings of Computer and Robot Vision* (2012).

[MZI13] Mosseri I., Zontak M., Irani M.: Combining the power of internal and external denoising. In *Proceedings of ICCP* (2013).

[NS06] Nistér D., Stewénius H.: Scalable recognition with a vocabulary tree. In *Proceedings of CVPR* (2006).

[OA12] Olonetsky I., Avidan S.: TreeCANN – k-d tree coherence approximate nearest neighbor algorithm. In *Proceedings of ECCV* (2012).

[PCI*07] Philbin J., Chum O., Isard M., Sivic J., Zisserman A.: Object retrieval with large vocabularies and fast spatial matching. In *Proceedings of CVPR* (2007).

[PM11] Pan J., Manocha D.: Fast GPU-based locality sensitive hashing for k-nearest neighbor computation. In *Proceedings of ACM SIGSPATIAL* (2011).

[QMN09] Qiu D., May S., Nüchter A.: GPU-accelerated nearest neighbor search for 3d registration. In *Proceedings of Computer Vision Systems* (2009).

[SAH08] Silpa-Anan C., Hartley R.: Optimised kd-trees for fast image descriptor matching. In *Proceedings of CVPR* (2008).

[TSPP14] Tsai Y.-T., Steinberger M., Pajak D., Pulli K.: Fast ANN for high-quality collaborative filtering. In *Proceedings of HPG* (2014).

[XLYD11] Xiao C., Liu M., Yongwei N., Dong Z.: Fast exact nearest patch matching for patch-based image editing and processing. *IEEE TVCG 17*, 8 (2011), 1122–1134.

[Yia93] YIANILOS P. N.: Data structures and algorithms for nearest neighbor search in general metric spaces. In *Proceedings of SODA* (1993).

[YLC13] YANG J., LIN Z., COHEN S.: Fast image super-resolution based on in-place example regression. In *Proceedings of CVPR* (2013).

[ZHWG08] ZHOU K., HOU Q., WANG R., GUO B.: Real-time kd-tree construction on graphics hardware. *ACM TOG 27*, 5 (2008), 126:1–126:11.

[ZI11] ZONTAK M., IRANI M.: Internal statistics of a single natural image. In Proceedings of CVPR (2011).

[Zit10] ZITNICK C. L.: Binary coherent edge descriptors. In *Proceedings of ECCV* (2010).